Energy Engineering

Tech Science Press

DOI: 10.32604/ee.2024.048161

ARTICLE

# Effect of Rigid Pitch Motion on Flexible Vibration Characteristics of a Wind Turbine Blade

**Zhan Wang[1], Liang Li[2,*], Long Wang[1], Weidong Zhu[3], Yinghui Li[4] and Echuan Yang[5]**

[1]School of Mechanical Engineering, Anhui University of Science and Technology, Huainan, 232001, China

[2]School of Mechanics and Optoelectronic Physics, Anhui University of Science and Technology, Huainan, 232001, China

[3]Department of Mechanical Engineering, University of Maryland, Baltimore, MD 21250, USA

[4]School of Mechanics and Aerospace Engineering, Southwest Jiaotong University, Chengdu, 610031, China

[5]School of Mechanical Engineering, Chongqing University of Technology, Chongqing, 400054, China

[*]Corresponding Author: Liang Li. Email: 2014060@aust.edu.cn

Received: 29 November 2023 Accepted: 24 July 2024 Published: 11 September 2024

## ABSTRACT

A dynamic pitch strategy is usually adopted to improve the aerodynamic performance of the blade of a wind turbine. The dynamic pitch motion will affect the linear vibration characteristics of the blade. However, these influences have not been studied in previous research. In this paper, the influences of the rigid pitch motion on the linear vibration characteristics of a wind turbine blade are studied. The blade is described as a rotating cantilever beam with an inherent coupled rigid-flexible vibration, where the rigid pitch motion introduces a parametrically excited vibration to the beam. Partial differential equations governing the nonlinear coupled pitch-bend vibration are proposed using the generalized Hamiltonian principle. Natural vibration characteristics of the inherent coupled rigid-flexible system are analyzed based on the combination of the assumed modes method and the multi-scales method. Effects of static pitch angle, rotating speed, and characteristics of harmonic pitch motion on flexible natural frequencies and mode shapes are discussed. It shows that the pitch amplitude has a dramatic influence on the natural frequencies of the blade, while the effects of pitch frequency and pith phase on natural frequencies are little.

## KEYWORDS

Pitch motion; wind turbine blade; inherent rigid-flexible coupling; vibration characteristics

## Nomenclature

| | |
|---|---|
| $A$ | Amplitude of the pitch motion |
| $\omega_p$ | Angular frequency of the pitch motion |
| $C$ | Initial phase of the pitch motion |
| $W$ | Flap displacement |
| $\theta_t$ | Pre-twist angle |
| $\theta_p$ | Pitch angle |
| $\Omega$ | Rotating speed |
| $\gamma$ | Modal function |
| $\overline{\omega}_i$ | Average frequency |
| $\omega_i$ | Natural frequency |

| | |
|---|---|
| $[\boldsymbol{K}]$ | Stiffness matrix |
| $[\boldsymbol{M}]$ | Mass matrix |
| r/min | Revolutions per minute |

## 1 Introduction

The study of the vibration characteristics of a blade is essential for the structural design and control of wind turbines. There has been a lot of work on linear or nonlinear vibrations of wind turbine blades. Chopra et al. [1] studied the parametrically excited vibration by simplifying a blade to a rotating rigid body. Larsen et al. [2–4] described a blade as a rotating Euler-Bernoulli beam with a coupled extension-bend-bend vibration and investigated the 1:2 internal resonance, parametric instability, and stochastic stability of the blade. Evans et al. [5] proposed a method to assess the fatigue life of small wind turbine blades operating at higher rotating speeds and subjected to highly unsteady aerodynamic loads and determine the fatigue life of small 5 kW wind turbine blades. Mahri et al. [6,7] used the finite element method (FEM) to calculate the frequency, mode, and forced vibration response of a blade. Liu et al. [8,9] reduced the blade to a composite thin-walled beam, considered the anisotropy of the material, cross-section warping, cone angle, pre-twist angle, and other factors, established a coupled bend-torsion vibration model, studied the flutter, dynamic characteristics, and aeroelastic response, and discussed the effects of fiber ply angle, inlet velocity ratio, pre-twist angle and rotating speed on the aeroelastic stability of the blade. Georgiades et al. [10] considered the factors of variable hub speed rotation, composite thin-walled structure, extension-bend-bend-torsion coupling, mounting angle, and section warping, and established a nonlinear dynamic model of the hub-beam system, where the aerodynamic effect was supplemented in the model, it can be directly applied to the vibration characteristics and stability of the wind wheel system. With the help of the model [10], Warminski et al. [11] employed the generalized Galerkin method to study the coupled extension-bend-torsion vibration of thin-walled composite beams with variable rotating speed and analyzed the dynamic characteristics of the beams including natural frequency, resonance response, and time history. Li et al. [12] introduced structural damping, gravity, inclined installation, and other factors into the model of a blade and analyzed the dynamical characteristics and nonlinear response of the blade. Chen et al. [13] studied the coupled bending-torsional vibration characteristics of the blade based on the transfer matrix method of a multibody system. For floating offshore wind turbines (FOWT), Fu et al. [14–18] used the finite element method and computational fluid dynamics (CFD) method, studied the dynamic characteristics of FOWT under pitch motion of platform, and concluded that the amplitude and frequency of pitch motion have a great influence on power output. Boudounit et al. [19] studied the structural design problem of offshore wind turbine blade spars based on the finite element method and discussed the influence of spars geometry on the blade performance including natural frequencies, modal shapes, and fatigue properties. Lagdani et al. [20] investigated the modal problem of an iced offshore composite wind turbine blade based on the finite element method and analyzed the influence of ice layer thickness and composite materials on natural frequencies and resonance. Previous literature provides a lot of important results and research methods for reference.

The pitch control strategy (the pitch motion is the rotation of a blade around the pitch axis, see Fig. 1; it is a rigid body motion) is usually used to improve the aerodynamic performance of a wind turbine blade. When the influences of the pitch motion are considered: Kallesøe [21] investigated the interaction of pitch, gravity, variable rotating speed, and blade vibration, and proposed a model of a blade with a pitch motion. Wang et al. [22–25] investigated the pitch control strategy to improve the performance of the blade. Seyednia et al. [26] studied the effect of flap trailing edge on airfoil dynamic stall control. Mahmoud et al. [27] performed continuous-time multi-model predictive control

for variable-speed variable-pitch wind turbines. Rainone et al. [28] developed a numerical program to determine the pitch law to maximize the performance of vertical axis wind turbines (VAWT). Sagharichi et al. [29] discussed the effect of solids on the performance of variable-pitch VAWT. Li et al. [30] analyzed the pitch optimization of a VAWT blade with a high tip speed ratio. Sendi [31] studied the power output of the variable pitch wind turbine at different wind speeds and discussed the output performance in the case of extreme gusts and long-period wind using blade element theory and the Lagrange equation.

The dynamic pitch motion can introduce a parametrically excited vibration to the blade, affect its flexible vibration characteristics, and may cause instability. However, research works referring to these influences of the pitch motion are rare. This paper aims to present a study on the influences of dynamic pitch motion on the natural bending characteristics of a blade.

## 2 Governing Equations

In this work, the out-of-plane bend (called flap) which usually has lower frequencies and larger displacement is considered. Fig. 1 shows the schematic diagrams of a wind turbine, a blade, and a cross-section. The angle between the flap direction and the chord line is the section twist angle $\theta = \theta_t + \theta_p$ (includes pre-twist angle $\theta_t$ and pitch angle $\theta_p$, see Fig. 1d). Cartesian right-handed systems [32,33] are employed to describe the configuration of the blade. $(xyz)$ with unit vectors $(\mathbf{i}, \mathbf{j}, \mathbf{k})$ is a body coordinate system that is rigidly attached to the blade root. The $x$-axis corresponds to the undeformed elastic axis, the $y$-axis lies in the plane of rotation, and the $z$-axis is along the flap direction. $(XYZ)$ with unit vectors $(\mathbf{I}, \mathbf{J}, \mathbf{K})$ is a global coordinate system with the origin at the center of mass of the hub. The $z$-axis is aligned with the spin axis backward, and the $y$-axis is parallel to the $y$-axis. Small cone angle $\beta_p$ between the rotation plane and the vertical plane is ignored in this work.

The blade is an elongated structure, which can be described as an Euler-Bernoulli beam. After blade deformation, the position vector of the point P $(x, y, z)$ can be calculated as [12,32,33]

$$\mathbf{OP} = (x+u)\,\mathbf{I} + (y - w\sin\theta)\,\mathbf{J} + (w\cos\theta + z)\,\mathbf{K}, \tag{1}$$

where $u$ is the axial displacement of the blade, and $w$ is the flap displacement. The velocity vector of the point P can be obtained from Eq. (1) as

$$\mathbf{v_P} = (\dot{u} + \Omega w\sin\theta - \Omega y)\,\mathbf{I} + \left[\Omega\,(u+x) - \dot{w}\sin\theta - w\dot{\theta}_p\cos\theta\right]\mathbf{J} + \left(\dot{w}\cos\theta - w\dot{\theta}_p\sin\theta\right)\mathbf{K}, \tag{2}$$

where dots denote derivatives to time $t$, $\Omega$ is the rotating speed of the blade. In the above equation, the equality $\dot{\theta} = \dot{\theta}_p$ is adopted. The variation of the kinetic energy $T$ [34] of the rotating blade is

$$\delta T = \frac{1}{2}\delta\left[\int_0^L \int_A \rho_b\,(\mathbf{v_P}\cdot\mathbf{v_P})\;\mathrm{d}A\mathrm{d}x + J_p\dot{\theta}_p^2\right], \tag{3}$$

where $L$ is the blade length, $\rho_b$ is the mass density per unit volume, $A$ is the cross-sectional area, and $J_p$ is the rotational inertia of the blade about the pitch axis. The shear strains $\gamma_{xy} = 0$, $\gamma_{xz} = 0$ can be assumed from the slender geometric characteristics of the blade. The strain $\varepsilon_x$ satisfies the nonlinear geometric relationship $\varepsilon_x = u' - rw'' + (1/2)\,(w')^2$ [32,33], where $r$ is the lateral distance from the point to the neutral axis, and primes represent derivatives to $x$. Based on the linear elastic stress-strain relationship $\sigma_x = E\varepsilon_x$, where $\sigma_x$ is the normal stress, and $E$ is Young's modulus, the variation of potential energy $U$ [34] can be written as

$$\delta U = \frac{1}{2}\delta\int_0^L \int_A E\varepsilon_x^2\mathrm{d}A\mathrm{d}x. \tag{4}$$

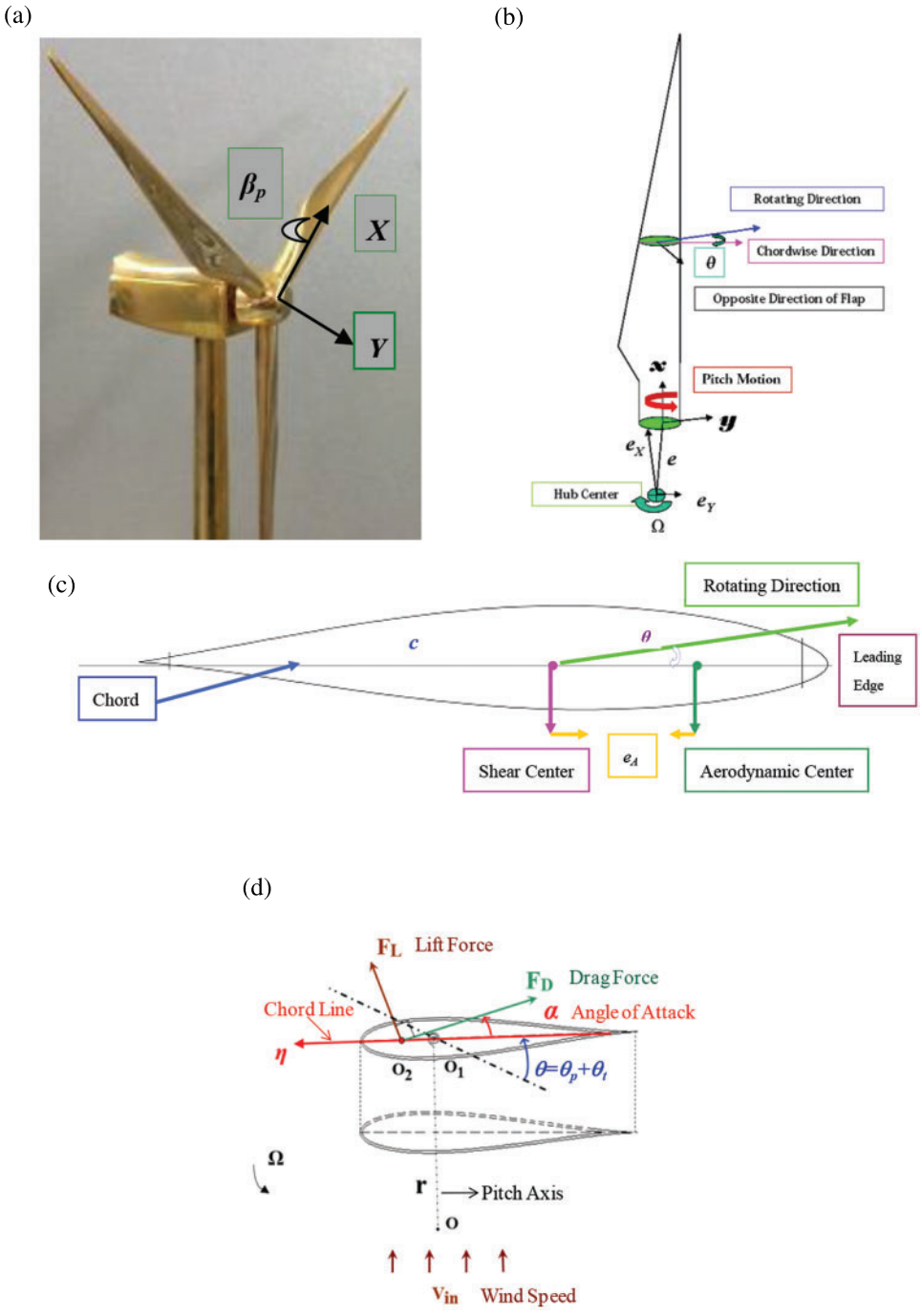


**Figure 1:** Diagram of (a) a wind turbine, (b) a pitching blade, (c) a section, and (d) section angles

The distributed external forces and moments acting in the flap direction on blade sections are denoted as $F_z$ and $M_y$, respectively. The resultant moment corresponding to the pitch motion is denoted as $M_p$, which includes the driving moment $E_p$ of the pitch mechanism, aerodynamic moment $A_p$, and structural damping moment $D_p$ of the pitch mechanism. The structural damping moment can

be equivalent to $D_p = -c_p\dot{\theta}_p$ using the damping coefficient $c_p$. The virtual work done by the external forces [34] can be written as

$$\delta W = \int_0^L \left(F_z \delta w + M_y \delta w'\right) \mathrm{d}x + M_p \delta\theta_p. \tag{5}$$

According to the generalized Hamiltonian principle [34], $\int_{t_1}^{t_2} (\delta T - \delta U + \delta W)\,\mathrm{d}t = 0$ holds for arbitrary $t_1$ and $t_2$. Governing equations of the inherently coupled flap-pitch motion of the blade can be obtained as

**Flap Vibration:**

$$(EIw'')'' - (F_T w')' + m\ddot{w} - mw\dot{\theta}_p^2 + m(u+x)\dot{\theta}_p \cos\theta - \frac{1}{2}\left[EA\,(w')^3\right]' = F_z - M_y',$$

i.e.,

$$\begin{aligned}&\left\{\left[EI_1\cos^2\left(\theta_p+\theta_t\right) + EI_2\sin^2\left(\theta_p+\theta_t\right)\right]w''\right\}'' - (F_T w')' + m\ddot{w}\\ &-mw\dot{\theta}_p^2 + m(u+x)\dot{\theta}_p\cos\left(\theta_p+\theta_t\right) - \frac{1}{2}\left[EA\,(w')^3\right]' = F_z - M_y',\end{aligned} \tag{6}$$

**Pitch Motion:**

$$\begin{aligned}&J_p\ddot{\theta}_p + mw^2\ddot{\theta}_p + 2mw\dot{w}\dot{\theta}_p - m\Omega\left(\dot{u}+x\right)w\cos\left(\theta_p+\theta_t\right) - m\Omega(u+x)\dot{w}\cos\left(\theta_p+\theta_t\right)\\ &+m\Omega(u+x)w\dot{\theta}_p\sin\left(\theta_p+\theta_t\right) = M_p = E_p + A_p + D_p,\end{aligned} \tag{7}$$

where $EI = EI_1\cos^2\left(\theta_p+\theta_t\right) + EI_2\sin^2\left(\theta_p+\theta_t\right)$ is the flapwise bending stiffness of the cross-section, $EI_1$ and $EI_2$ are the first and second principal stiffness of the cross-section, respectively, $m$ is the mass of the cross-section, and $F_T = \int_x^L m(y)\,\Omega^2(e+y)\,dy$ is the centrifugal force of the cross-section. From Eq. (6) one finds that the influence of pitch motion on flap vibration is mainly on elastic restoring force, Coriolis force, excitation, and aerodynamic forces. The pitch rule $\theta_p = \theta_p(t)$ is usually obtained by considering the aerodynamic performance of the blade. The pitch controlling is executed through driving moment $E_p$ based on Eq. (7) and the pitch rule. To obtain the natural vibration characteristics of the blade, one considers the linearly undamped vibration of the blade with the following equations:

**Flap Vibration:**

$$\left\{\left[EI_1\cos^2\left(\theta_p+\theta_t\right) + EI_2\sin^2\left(\theta_p+\theta_t\right)\right]w''\right\}'' - (F_T w')' + m\ddot{w} = 0. \tag{8}$$

Based on Fourier's theory, a complicated signal can be expressed as the superposition of a series of harmonic signals. Therefore, we consider the simple harmonic signal in this paper first.

## 3 Analysis of Free Vibration of the Inherent Coupled Rigid-Flexible System

Bending stiffness $EI$ changes with time-dependent pith angle $\theta_p = \theta_p(t)$, so the linear modal problem of the blade with a dynamic pitch motion (see Eq. (8)) is different from a routine one (for a beam with constant bending stiffness and mass). A combination method based on the assumed modes method [34] and multi-scales method [35] is proposed to solve the problem, and then the required natural frequencies are calculated. Without loss of generality, we neglect the pre-twist angle $\theta_t$. The

undamped free vibration problem (8) can be rewritten as

$$\left(\left(\frac{EI_1+EI_2}{2}+\frac{(EI_1-EI_2)}{2}\cos 2\theta_p\right)w''\right)''-F_Tw''+m\ddot{w}=0. \tag{9}$$

Here we assume $\cos 2\theta_p$ changes periodically with time; it can be expressed to the following Fourier series:

$$\cos 2\theta_p=\sum_{n=-\infty}^{\infty}\hat{X}_n e^{in\omega_p t},\ \hat{X}_n=\varepsilon X_n, \tag{10}$$

where i is the complex unit, $\varepsilon$ is a small parameter. By substituting Eq. (10) into Eq. (9), one obtains the following equation:

$$\left[\left(\frac{EI_1+EI_2}{2}+\frac{EI_1-EI_2}{2}\varepsilon\sum_{n=-\infty}^{\infty}X_n e^{in\omega_p t}\right)w''\right]''-F_Tw''+m\ddot{w}=0. \tag{11}$$

Introducing two time scales $T_0=t$ and $T_1=\varepsilon t$ and assuming:

$$w(x,t,\varepsilon)=w_0(x,T_0,T_1)+\varepsilon w_1(x,T_0,T_1)+O\left(\varepsilon^2\right). \tag{12}$$

By substituting Eq. (12) into Eq. (11), one has

$$\begin{aligned}&\left[\left(\frac{EI_1+EI_2}{2}+\frac{EI_1-EI_2}{2}\varepsilon\sum_{n=-\infty}^{\infty}X_n e^{in\omega_p t}\right)(w_0+\varepsilon w_1)''\right]''-F_T(w_0+\varepsilon w_1)''\\&+m\left(D_0^2w_0+2\varepsilon D_0D_1w_0+\varepsilon^2D_1^2w_0+\varepsilon D_0^2w_1+2\varepsilon^2D_0D_1w_1+\varepsilon^3D_1^2w_1\right)=0\end{aligned}. \tag{13}$$

When considering the coefficients of $\varepsilon^0$ in Eq. (13), one has

$$\left(\frac{EI_1+EI_2}{2}{w_0}''\right)''-F_T{w_0}''+m{D_0}^2w_0=0. \tag{14}$$

If considering the coefficients of $\varepsilon^1$ in Eq. (13), one obtains

$$\left(\frac{EI_1+EI_2}{2}{w_1}''\right)''+\left(\frac{EI_1-EI_2}{2}\sum_{n=-\infty}^{\infty}X_n e^{in\omega_p t}{w_0}''\right)''-F_T(w_1)''+m\left(2D_0D_1w_0+D_0^2w_1\right)=0. \tag{15}$$

By assuming $w_0=A(T_1)e^{i\omega T_0}\gamma(x)+c.c.$ and substituting it into Eq. (14), one derives the following equation:

$$\left(\frac{EI_1+EI_2}{2}\gamma''(x)\right)''-F_T\gamma(x)''-m\omega^2\gamma(x)=0, \tag{16}$$

where *c.c.* represents the conjugate of the preceding function. The approximate boundary conditions are

$$\gamma(x)|_{x=0}=0,\gamma'(x)|_{x=0}=0,\ \left(\frac{EI_1+EI_2}{2}\gamma''(x)\right)|_{x=L}=0,\ \left(\frac{EI_1+EI_2}{2}\gamma''(x)\right)'|_{x=L}=0. \tag{17}$$

Exact solutions of Eq. (16) cannot be obtained directly. The assumed modes method is adopted to solve the problem [34]. By taking a family of trail functions that satisfy the geometry boundary

conditions $\{\Phi_1(x), \Phi_2(x), \cdots, \Phi_n(x)\}$, the modal function is expressed as

$$\gamma(x) = \sum_{i=1}^{n} A_i \Phi_i(x). \tag{18}$$

By substituting Eq. (18) into Eq. (16), multiplying $\Phi_j(x)$ at both ends together and then integrating $x$ from 0 to $L$, a set of algebraic equations about unknown constants $A$ is determined as follows:

$$\left([K] - \overline{\omega}^2 [M]\right) A = \{0, 0, \cdots, 0\}^T, \tag{19}$$

where

$$[K] = \begin{bmatrix} k_{11} & k_{12} & \cdots & k_{1n} \\ k_{21} & k_{22} & \cdots & k_{2n} \\ \vdots & \vdots & \vdots & \vdots \\ k_{n1} & k_{n2} & \cdots & k_{nn} \end{bmatrix}, \quad [M] = \begin{bmatrix} m_{11} & m_{12} & \cdots & m_{1n} \\ m_{21} & m_{22} & \cdots & m_{2n} \\ \vdots & \vdots & \vdots & \vdots \\ m_{n1} & m_{n2} & \cdots & m_{nn} \end{bmatrix}$$

$A = \{A_1, A_2, \cdots, A_n\}^T$, the elements of stiffness matrix $[K]$ and mass matrix $[M]$ are

$$m_{ij} = \int_0^L m \Phi_i \Phi_j \mathrm{d}x,$$

$$k_{ij} = \int_0^L EI \Phi_i'' \Phi_j'' \mathrm{d}x + \int_0^L \int_x^L m\Omega^2 \left(e + y\cos\beta_p\right) \mathrm{d}y \, \Phi_i' \Phi_j' \mathrm{d}x,$$

The algebraic Eq. (19) has non-zero solutions, so one has

$$\left|[K] - \overline{\omega}^2 [M]\right| = 0. \tag{20}$$

One can derive the $i$th-order average frequency $\overline{\omega}_i$ and the modal function $\gamma_i$ from Eqs. (20) and (19). Substituting the expression of $w_0$ into Eq. (15), one has

$$\begin{aligned} &\left(\frac{EI_1 + EI_2}{2} {w_1}''\right)'' - F_T (w_1)'' + mD_0^2 w_1 \\ &= -2mD_0 D_1 w_0 - \left(\frac{EI_1 - EI_2}{2} \sum_{n=-\infty}^{\infty} X_n \mathrm{e}^{\mathrm{i}n\omega p t} {w_0}''\right)'' \\ &= -2m\mathrm{i}\omega \mathrm{e}^{\mathrm{i}\overline{\omega} T_0} \gamma(x) D_1 A - \left(\frac{EI_1 - EI_2}{2} \overline{A} \gamma''(x) \sum_{n=-\infty}^{\infty} X_n \mathrm{e}^{\mathrm{i}\left(n\omega p - \overline{\omega}\right) T_0}\right)'' + c.c. \end{aligned} \tag{21}$$

In the case of non-resonance, i.e., the pitch frequency and the average frequency have no resonance, the condition of eliminating the long-term term introduces

$$-2m\mathrm{i}\overline{\omega}\gamma(x) D_1 A - \left(\frac{EI_1 - EI_2}{2} A X_0 \gamma''(x)\right)'' = 0. \tag{22}$$

Both sides of Eq. (22) are multiplied $\gamma(x)$ at the same time, and integrated $x$ from 0 to $L$, one has

$$\int_0^L \left[-2m\mathrm{i}\overline{\omega}\gamma(x) D_1 A - \left(\frac{EI_1 - EI_2}{2} A X_0 \gamma''(x)\right)''\right] \gamma(x) \, dx = 0, \tag{23}$$

where $A(T_1) = \frac{1}{2}ae^{i\beta}$ and $D_1A = \frac{1}{2}(D_1a + iaD_1\beta)e^{i\beta}$. Substituting these two expressions into Eq. (23), one obtains

$$\int_0^L [-mi\overline{\omega}\gamma(x)(D_1a + iaD_1\beta)]\gamma(x)dx - \int_0^L \left[\frac{EI_1 - EI_2}{4}aX_0\gamma''(x)\right]''\gamma(x)dx = 0. \tag{24}$$

By separating the real and imaginary parts of Eq. (24), one has

$$\int_0^L m\overline{\omega}aD_1\beta\gamma^2(x)dx - \int_0^L \left[\frac{EI_1 - EI_2}{4}aX_0\gamma''(x)\right]''\gamma(x)dx = 0,$$

$$\int_0^L -m\overline{\omega}\gamma^2(x)D_1adx = 0.$$

After simplification, the following equations are obtained:

$$D_1\beta = \frac{\int_0^L [(EI_1 - EI_2)\gamma''(x)]''\gamma(x)dx}{4\int_0^L m\overline{\omega}\gamma^2(x)dx}X_0, \tag{25}$$

$$D_1a = 0. \tag{26}$$

Solving $a$ and $\beta$ from Eqs. (25) and (26), one has

$$a = C, \quad \beta = \frac{\int_0^L [(EI_1 - EI_2)\gamma''(x)]''\gamma(x)dx}{4\int_0^L m\overline{\omega}\gamma^2(x)dx}X_0T_1 + \beta_0. \tag{27}$$

The following formula can be obtained:

$$A(T_1) = \frac{1}{2}Ce^{i(QX_0+\beta_0)}, \quad Q = \frac{\int_0^L [(EI_1 - EI_2)\gamma''(x)]''\gamma(x)dx}{4\int_0^L m\overline{\omega}\gamma^2(x)dx},$$

$$w_0 = \frac{1}{2}Ce^{i(QX_0T_1+\beta_0+\omega T_0)}\gamma(x) + c.c. = C\cos[(Q\varepsilon X_0 + \omega)t + \beta]\gamma(x).$$

By truncating $w$ at $\varepsilon^0$, the approximate solution of $w$ is obtained:

$$w \approx w_0 = \frac{1}{2}Ce^{i(QX_0T_1+\beta_0+\omega T_0)}\gamma(x) = C\cos[(Q\varepsilon X_0 + \overline{\omega})t + \beta]\gamma(x), \tag{28}$$

where constants $C$ and $\beta_0$ can be determined by the initial conditions. When there is no resonance between pitch motion and blade vibration, the $i$th-order flapwise natural frequency of a dynamically pitching blade is $\omega_i = (Q\varepsilon X_0 + \overline{\omega}_i)$.

## 4 Effect of Rigid Pitch Motion on Flexible Natural Characteristics

### *4.1 Validation of the Theoretical Method*

The method proposed in Section 3 is suitable for arbitrary pitching beam structures, not limited to wind turbine blades. In this section, the theoretical method introduced in this work is validated by selecting a rotating cantilever beam model with rectangular cross sections and the following parameters: the length $L = 3$ m, width $b = 0.3$ m, height $h = 0.2$ m, Young's modulus $E = 210$ GPa, density $\rho = 7.8 \times 10^3$ kg/m$^3$, two principal moments of inertia of cross section$I_1 = bh^3/12$ and $I_2 = b^3h/12$, mass of the cross-section $m = \rho bh$. Results derived from the current method are compared with

the results that are obtained based on the single assumed modes method (AMM) and the finite element method (FEM). Here, the time-independent pitch angle is considered because the single AMM and the FEM cannot deal with the dynamic pitch problem. Four polynomial functions $\Phi_1 = (x/L)^2$, $\Phi_2 = (x/L)^3$, $\Phi_3 = (x/L)^4$, $\Phi_4 = (x/L)^5$ that satisfy the geometric boundary conditions are taken as trail functions in the AMM and current method. The finite element analysis is conducted by using the commercial ANSYS software, where boundary conditions are added to the section $x = 0$ such that the beam can rotate about the $z$-axis freely and other displacements of the section $x = 0$ are fixed to be zero. Solid186 element is used to mesh the structure, where the number of nodes is 621 and the number of elements is 80. Results of the current method are obtained by using the formula $\omega_i = (Q\varepsilon X_0 + \overline{\omega}_i)$.

The first three flapwise natural frequencies of the beam at zero rotating speed and zero pitch angle are presented in Table 1. Exact frequencies can be obtained directly in this case. The relative error is defined as $(\omega_{\text{Method}} - \omega_{\text{Exact Result}})/\omega_{\text{Exact Result}}$ to reveal the accuracy of the three methods. One finds from Table 1 that the results of the three methods coincide with the exact results well, especially for the AMM results. Results derived from the current method coincide with exact results well even though the accuracy of the current method is a little bit lower than those of another two methods; the current method provides an effective tool to solve the natural vibration characteristics of a dynamically pitching blade or beam. The first three flapwise frequencies with unit Hz and mode shapes which are obtained from FEM are shown in Fig. 2.

**Table 1:** The first three flapwise natural frequencies, where $\Omega = 0$ r/min and $\theta_p = 0°$

| Frequency (rad/s) | Exact result | AMM | Error (%) | FEM | Error(%) | Current method | Error (%) |
|---|---|---|---|---|---|---|---|
| $\omega_1$ | 117.02 | 117.03 | 0.00 | 117.33 | 0.26 | 120.50 | 2.97 |
| $\omega_2$ | 733.41 | 737.54 | 0.06 | 720.74 | −1.73 | 759.39 | 3.54 |
| $\omega_3$ | 2053.77 | 2108.55 | 2.67 | 1958.41 | −4.64 | 2170.99 | 5.71 |

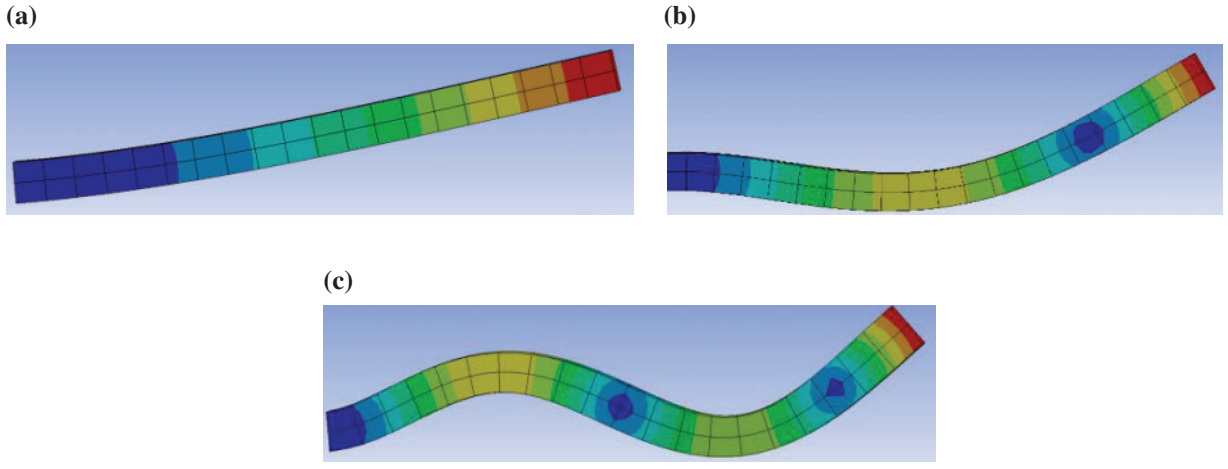


**Figure 2:** The (a) first-order, (b) second-order, and (c) third-order modal functions

The first three flapwise natural frequencies of the beam with rotating speed $\Omega = 150$ r/min and zero pitch angle are illustrated in Table 2, while exact frequencies can not be calculated directly in this

case. Results obtained from the current method are compared with AMM results and FEM results. The relative error is defined as $(\omega_{\text{Current Method}} - \omega_{\text{Other Method}})/\omega_{\text{Other Method}}$ to reveal the accuracy of the current method. It shows that the current results coincide with the AMM results very well. When the current method is compared with the FEM, there is a little bit higher error occurs at the third frequency due to the lower accuracy of both the FEM and current method at higher modes, see Table 1.

**Table 2:** The first three flapwise natural frequencies, where $\Omega = 150$ r/min and $\theta_p = 0°$

| Frequency (rad/s) | Current method | AMM | Error (%) | FEM | Error (%) |
|---|---|---|---|---|---|
| $\omega_1$ | 122.77 | 119.45 | 2.78 | 118.5 | 3.60 |
| $\omega_2$ | 761.94 | 740.27 | 2.93 | 721.38 | 5.62 |
| $\omega_3$ | 2173.23 | 2110.96 | 2.95 | 1958.36 | 10.97 |

Table 3 provides the first three flapwise natural frequencies of the beam with a constant pitch angle $\theta_p = 20°$ at two different rotating speeds $\Omega = 0$ and $\Omega = 150$ r/min. The FEM can not be used to calculate frequencies in this case. The current results are compared with the AMM results, where the relative error is defined as $(\omega_{\text{Current Method}} - \omega_{\text{AMM}})/\omega_{\text{AMM}}$. One finds from Table 3 that results derived from the two methods coincide with each other pretty well.

**Table 3:** The first three flapwise natural frequencies when $\theta_p = 20°$

| Frequency (rad/s) | $\Omega = 0$ r/min | | | $\Omega = 150$ r/min | | |
|---|---|---|---|---|---|---|
| | AMM | Current method | Error (%) | AMM | Current method | Error (%) |
| $\omega_1$ | 125.30 | 127.21 | 1.52 | 127.56 | 129.40 | 1.44 |
| $\omega_2$ | 789.63 | 801.69 | 1.53 | 792.18 | 804.14 | 1.51 |
| $\omega_3$ | 2257.45 | 2291.92 | 1.53 | 2259.70 | 2294.08 | 1.52 |

### *4.2 Effect of Rigid Pitch Motion on Flexible Natural Characteristics*

Take the megawatt (MW) wind turbine blade in reference [12] as an example, where distributions of chord length, thickness, and moments of inertia are shown in Fig. 3. Blade length $L = 48$ m, elastic modulus $E$ is 30 GPa, blade density $\rho_b = 1.8 \times 10^3$ kg/m$^3$, bias $(eX, eY) = (0.035, 0.035) \times L$. Four polynomial functions $\Phi_1 = (x/L)^2$, $\Phi_2 = (x/L)^3$, $\Phi_3 = (x/L)^4$, $\Phi_4 = (x/L)^5$ that satisfy the geometric boundary conditions are taken as trail functions. The accuracy of the results is validated by the AMM results, where two different rotating speeds $\Omega = 0$ and $\Omega = 15$ r/min are taken. The first three flapwise natural frequencies of the blade with a constant pitch angle $\theta_p = 20°$ are shown in Table 4. It reveals that results derived from the two methods coincide pretty well.

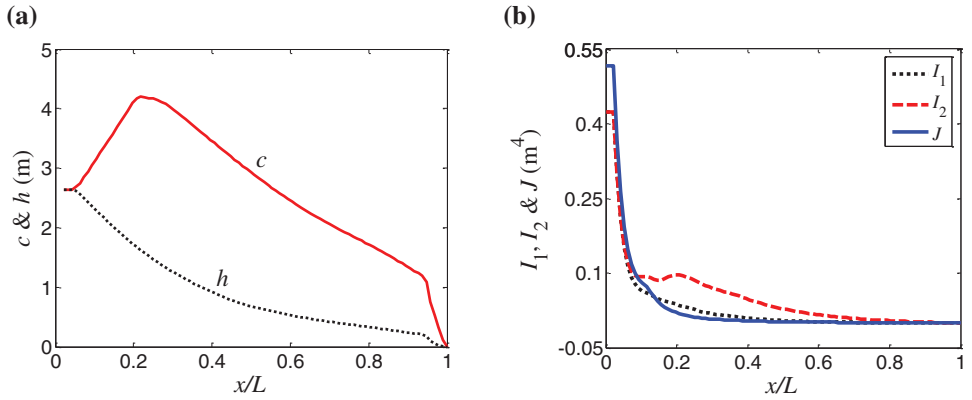


**Figure 3:** Distributions of (a) the chord length $c$, thickness $h$, and (b) three moments of inertia $I_1$, $I_2$, and $J$

**Table 4:** The first three flapwise natural frequencies of the blade when $\theta_p = 2°$

| Frequency (rad/s) | $\Omega = 0$ r/min | | | $\Omega = 15$ r/min | | |
|---|---|---|---|---|---|---|
| | AMM | Current method | Error (%) | AMM | Current method | Error (%) |
| $\omega_1$ | 1.30 | 1.33 | 2.31 | 3.20 | 3.28 | 2.5 |
| $\omega_2$ | 3.05 | 3.07 | 0.66 | 9.53 | 9.59 | 0.63 |
| $\omega_3$ | 27.01 | 27.06 | 0.19 | 27.62 | 27.65 | 0.11 |

Influences of constant pitch angles on average frequencies and modal functions of the blade are studied first. The first three average frequencies at three different rotating speeds 10, 20, and 30 r/min are presented in Fig. 4. One finds that average frequencies increase with increasing rotating speed, which is because increasing rotating speed can increase the blade stiffness through centrifugal force, which coincides with results in [36–38]; the variation of pitch angle also changes the natural frequencies of the blade.

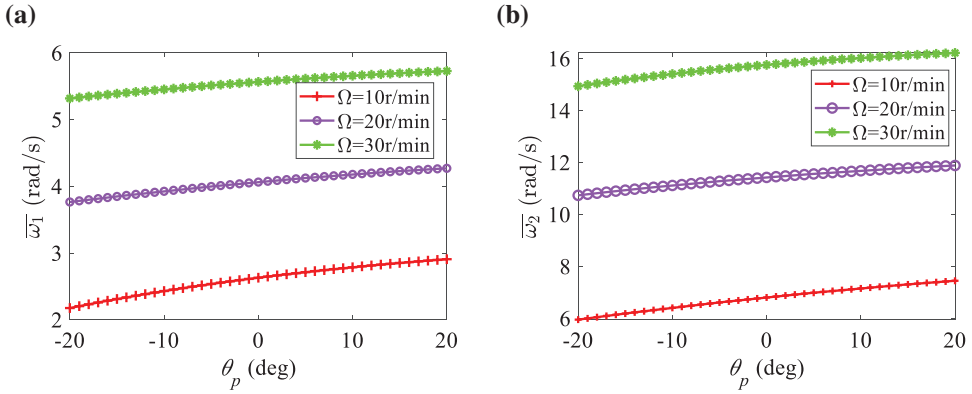


**Figure 4:** (Continued)

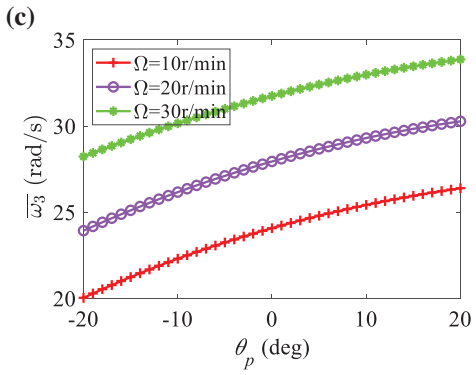


**Figure 4:** Effect of pitch angle on the average frequency at different rotating speeds: (a) first-order frequency; (b) second-order frequency; (c) third-order frequency

Effects of rotating speed on the first three modal functions are presented in Fig. 5 by selecting a fixed pitch angle $\theta_p = 2°$ and five different rotating speeds $\Omega = 0$, 5, 10, 15, and 20 r/min. The value of each modal function at the blade tip has been set to 1. It reveals that the rotating speed has dramatic influences on modal functions. Increasing the rotating speed makes the first-order and third-order modal shapes steeper, while it is contrary to the second-order modal shape. Influences of pitch angle $\theta_p$ on the first three modal functions are given in Fig. 6 by taking a fixed rotating speed $\Omega = 15$ r/min and five different pitch angles $\theta_p = -10°$, $-5°$, 0°, 5°, and 10°. One finds that the influence of pitch angle on each modal function is very small. The natural characteristics of a blade at special pitch rules are discussed in the following part.

In this part, a harmonic pitch motion $\theta_p = A\sin(\omega_p t + C)$ is adopted in analysis, where $A$, $\omega_p$, and $C$ are the amplitude, angular frequency, and initial phase of the pitch angle with units deg, rad/s, and rad, respectively.

The natural frequency $\omega_i = (Q\varepsilon X_0 + \overline{\omega}_i)$of the parametrically excited system has been obtained from Eq. (28). By calculating the average frequency $\overline{\omega}_i$ when the rotating speed $\Omega = 15$ r/min, one can discuss the influences of pitch parameters including $A$, $\omega_p$, and $C$ on natural frequencies.

Fig. 7 shows that when the values of pitch frequency $\omega_p$ change, each natural frequency varies with pitch amplitude $A$ dramatically. Fig. 8 presents the variation of frequency with pitch amplitude $A$ when pitch phase $C$ is taken as $\pi/4$ rad, $\pi/2$ rad, and $\pi$ rad, respectively. It can be seen from Figs. 7 and 8 that the frequency changes with the pitch amplitude $A$: when the value of $A$ is 110°, the frequency reaches the maximum, and then begins to change like an attenuation vibration; it reaches the second peak at $A = 290°$. It can also be seen that different values of pitch frequency $\omega_p$ and pitch phase $C$ do not affect the natural frequencies.

Fig. 9 shows that when the values of pitch amplitude $A$ change, the frequency varies with the pitch frequency $\omega_p$. Fig. 10 reveals the variation of each frequency with the pitch frequency $\omega_p$ when pitch phase $C$ is taken as $\pi/4$ rad, $\pi/2$ rad, and $\pi$ rad, respectively. Fig. 11 illustrates that when the values of pitch amplitude $A$ are different, the frequency varies with the pitch phase $C$. Fig. 12 shows the variation of each frequency with the pitch phase $C$ when pitch frequency $\omega_p$ is taken as 1/2 rad/s, 3 rad/s, 5 rad/s, and $\pi$ rad/s, respectively.

It is found from Figs. 9 to 12 that the frequency does not change with the pitch frequency $B$ and pitch phase $C$. However, the change in the value of the pitch amplitude $A$ is different. It can be seen

from Figs. 9 and 11 that when the value of the pitch amplitude $A$ is 5°, 15°, 30°, and 60°, respectively, the frequency does not change with the pitch frequency $\omega_p$ and pitch phase $C$, but its value increases, and Figs. 10 and 12 show that the values both of the pitch frequency $\omega_p$ and pitch phase $C$ do not change the values of frequencies. The results are consistent with the conclusions of Figs. 7 and 8.

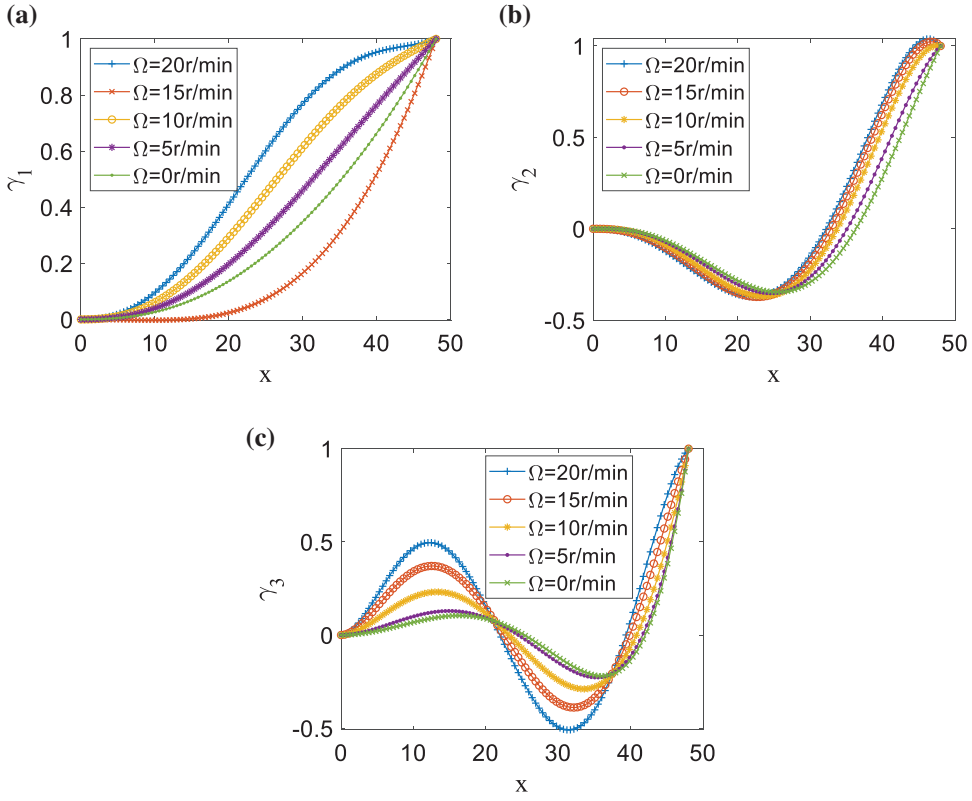


**Figure 5:** Influences of rotating speed $\Omega$ on (a) first-order, (b) second-order, and (c) third-order modal functions, where $\theta_p = 2°$

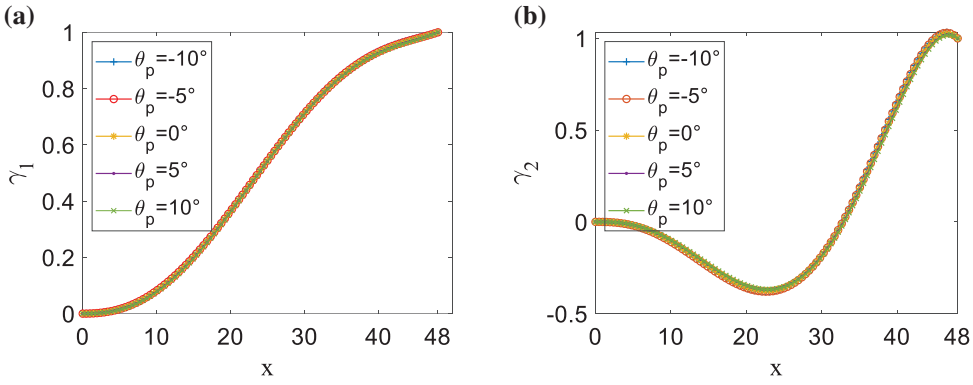


**Figure 6:** (Continued)

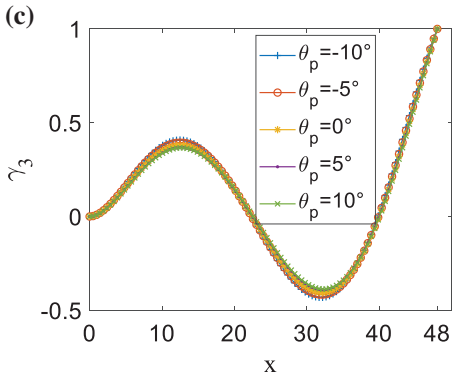


**Figure 6:** Influences of pitch angle $\theta_p$ on (a) first-order, (b) second-order, and (c) third-order modal functions, where $\Omega = 15$ r/min

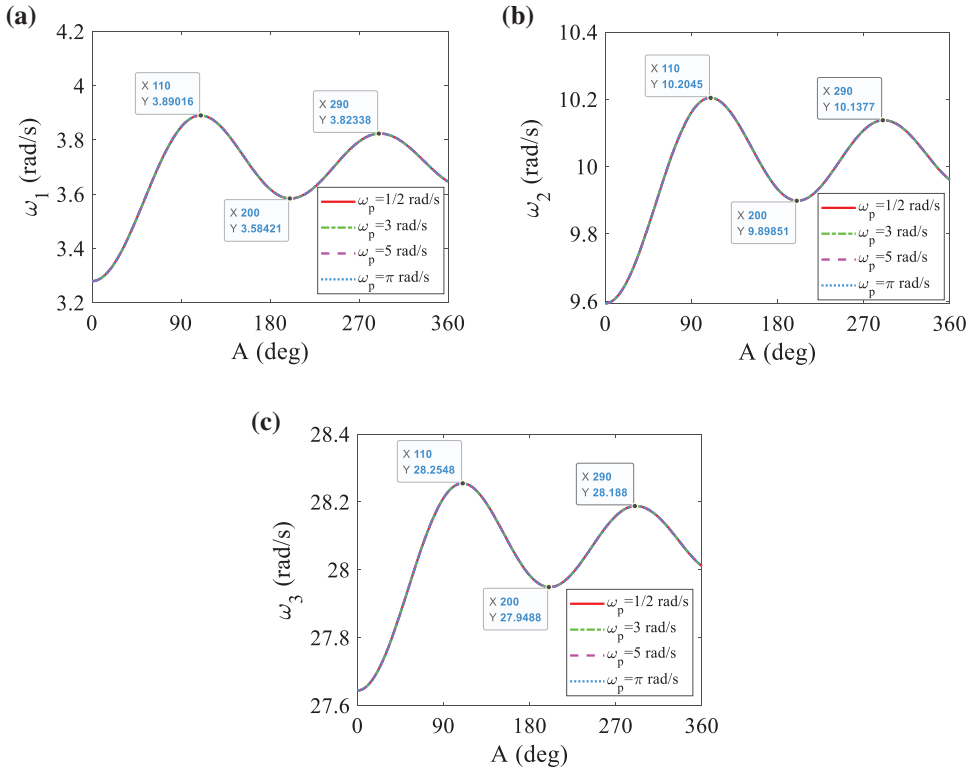


**Figure 7:** The influence of pitch amplitude $A$ on frequency under different pitch frequency $\omega_p$: (a) first-order frequency; (b) second-order frequency; (c) third-order frequency, where $C = 0$ rad

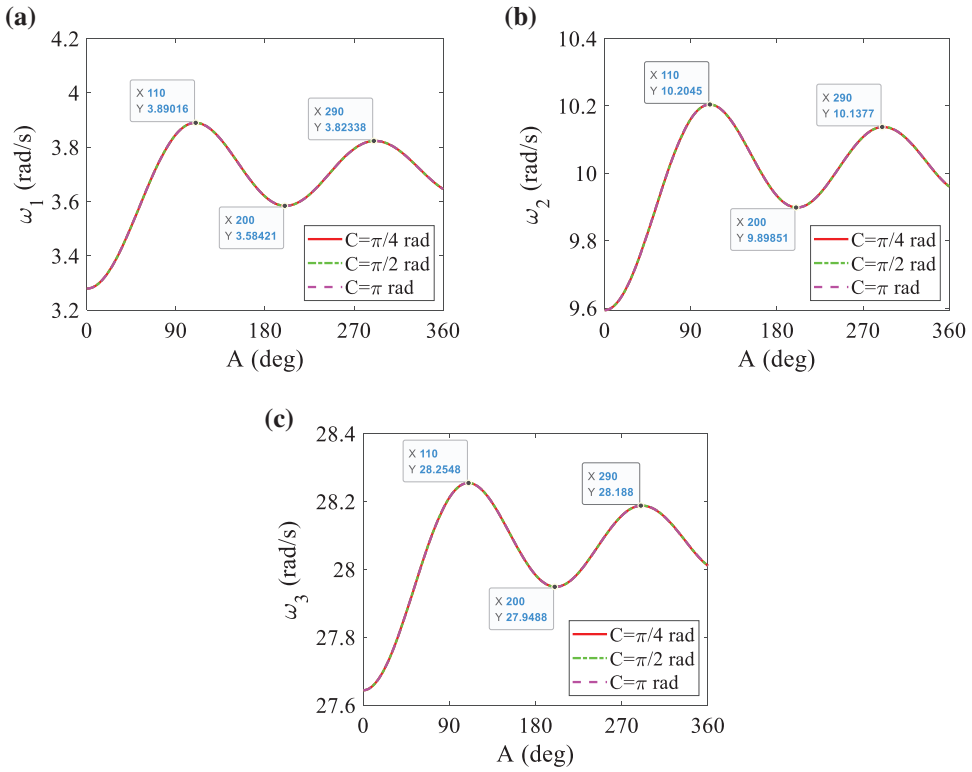


**Figure 8:** The influence of pitch amplitude $A$ on frequency under different pitch phase $C$: (a) first-order frequency; (b) second-order frequency; (c) third-order frequency, where $\omega_p = 1/2$ rad/s

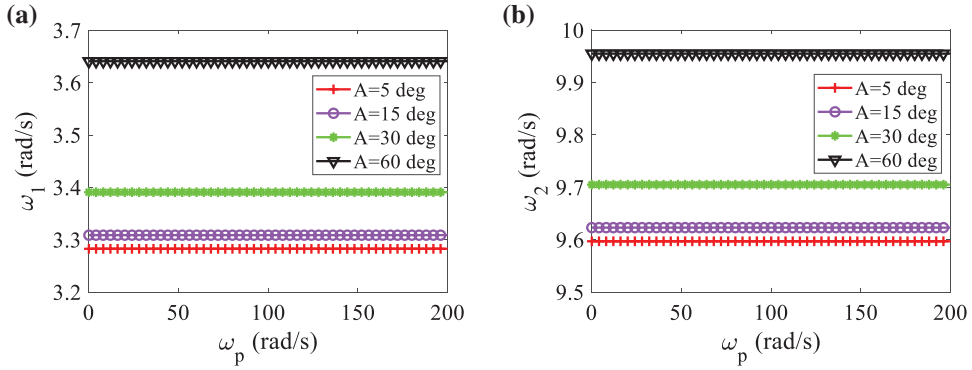


**Figure 9:** (Continued)

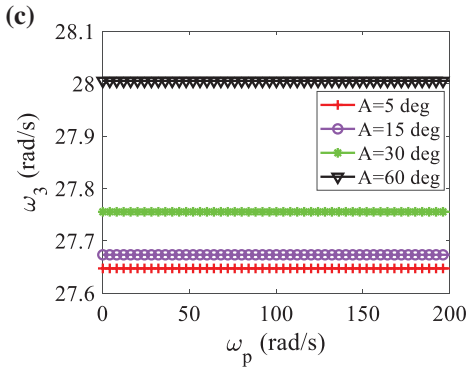


**Figure 9:** The influence of pitch frequency $\omega_p$ on frequency under different pitch amplitude $A$: (a) first-order frequency; (b) second-order frequency; (c) third-order frequency, where $C = 0$ rad

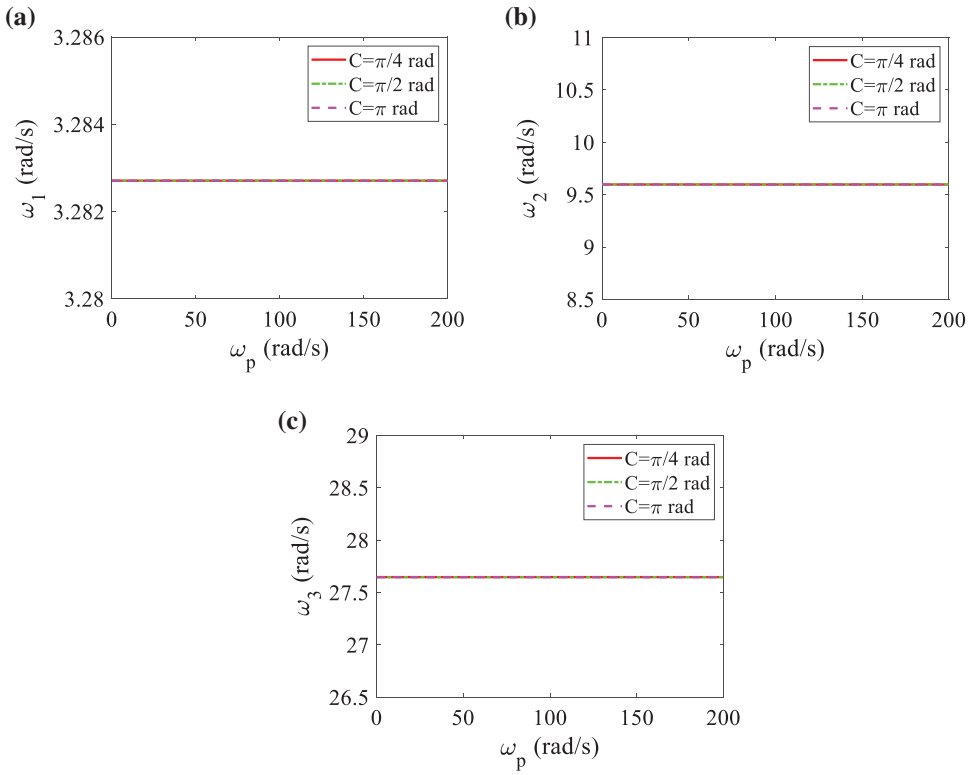


**Figure 10:** The influence of pitch frequency $\omega_p$ on frequency under different pitch phase $C$: (a) first-order frequency; (b) second-order frequency; (c) third-order frequency, where $A = 5°$

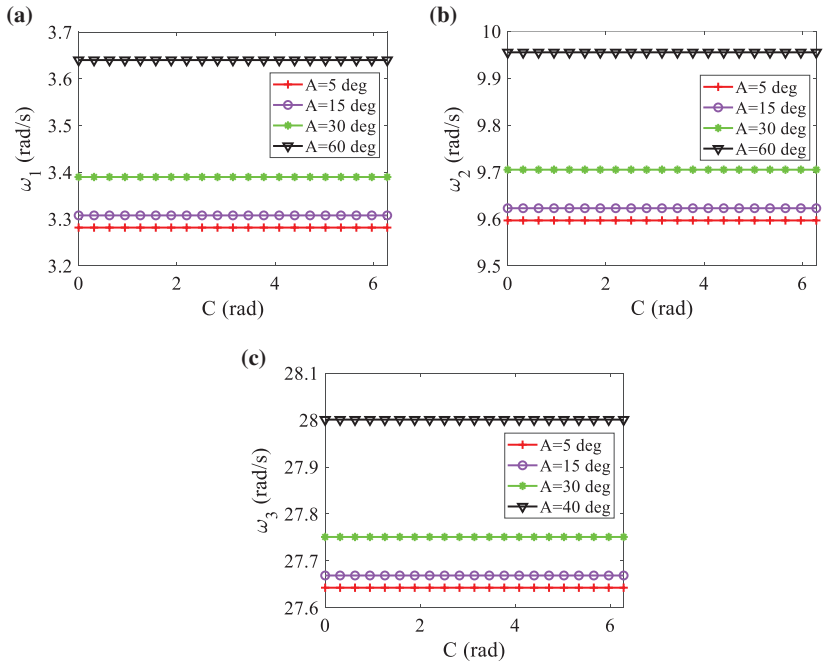


**Figure 11:** The influence of pitch phase $C$ on frequency under different pitch amplitude $A$: (a) first-order frequency; (b) second-order frequency; (c) third-order frequency, where $\omega_p = 1/2$ rad/s

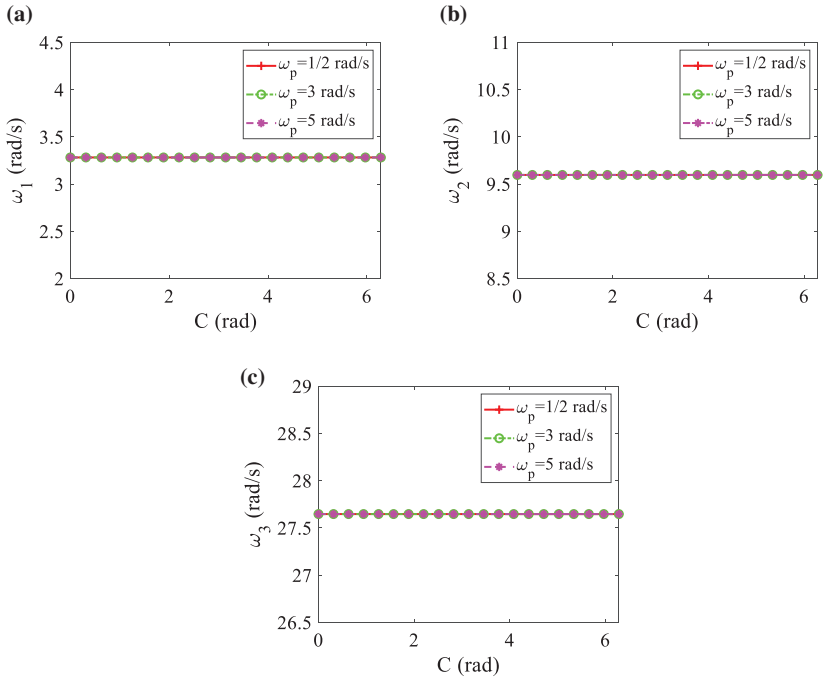


**Figure 12:** The influence of pitch phase $C$ on frequency under different pitch frequency $\omega_p$: (a) first-order frequency; (b) second-order frequency; (c) third-order frequency, where $A = 5°$

## 5 Conclusions

In this paper, the influence of rigid pitch motion on flexible vibration characteristics of a wind turbine blade was studied. A nonlinear inherent coupled rigid-flexible dynamic model of a pitching blade is derived based on the generalized Hamiltonian principle. The combination of the assumed modes method and the multi-scales methods was proposed to deal with the linear modal problem. Natural characteristics of the blade with a harmonic pitch motion were analyzed. Effects of pitch motion on natural frequencies and mode shapes were analyzed. The following conclusions were obtained: (1) static pitch angle has little influence on the first three mode shapes for fixed rotating speed; (2) the amplitude of dynamic pitch motion influences the first three natural frequencies dramatically, while the influence of pitch frequency and pitch phase on natural frequencies is tiny; (3) the influence of dynamic pitch angle on vibration characteristics of the blade is very different from that of static pitch angle, so the conclusions for static pitch angle cannot be used to a dynamically pitching blade directly when vibration characteristics problem is considered; (4) natural frequencies increase with increasing rotating speed due to the centrifugal hardening effect.

**Acknowledgement:** None.

**Funding Statement:** This work has been supported by the University Outstanding Youth Researcher Support Program of the Education Department of Anhui Province, the National Natural Science Foundation of China (Grant Nos. 11902002 and 51705002), the Sichuan Provincial Natural Science Foundation (Grant No. 2022NSFSC0275), the Science and Technology Research Project of Chongqing Municipal Education Commission (Grant No. KJQN201901146) and the Special Key Project of Technological Innovation and Application Development in Chongqing (Grant No. cstc2020jscx-dxwtBX0048).

**Author Contributions:** The authors confirm contribution to the paper as follows: study conception and design: Zhan Wang, Liang Li; data collection: Zhan Wang, Long Wang; analysis and interpretation of results: Zhan Wang, Liang Li, Long Wang, Weidong Zhu, Yinghui Li, Echuan Yang; draft manuscript preparation: Zhan Wang, Liang Li, Weidong Zhu, Yinghui Li, Echuan Yang. All authors reviewed the results and approved the final version of the manuscript.

**Availability of Data and Materials:** The datasets used or analyzed during the current study are available from the corresponding author upon reasonable request.

**Ethics Approval:** Not applicable.

**Conflicts of Interest:** The authors declare that they have no conflicts of interest to report regarding the present study.

## References

[1] I. Chopra and J. Dugundji, "Non-linear dynamic response of a wind turbine blade," *J. Sound Vib.*, vol. 63, no. 2, pp. 265–286, Mar. 1979. doi: 10.1016/0022-460X(79)90883-6.

[2] J. W. Larsen and S. R. K. Nielsen, "Non-linear dynamics of wind turbine wings," *Int. J. Nonlin. Mech.*, vol. 41, no. 5, pp. 629–643, Jun. 2006. doi: 10.1016/j.ijnonlinmec.2006.01.003.

[3] J. W. Larsen and S. R. K. Nielsen, "Nonlinear parametric instability of wind turbine wings," *J. Sound Vib.*, vol. 299, no. 1–2, pp. 64–82, Jan. 2007. doi: 10.1016/j.jsv.2006.06.055.

[4] J. W. Larsen, R. Iwankiewicz, and S. R. K. Nielsen, "Nonlinear stochastic stability analysis of wind turbine wings by Monte Carlo simulations," *Probabilist Eng. Mech.*, vol. 22, no. 2, pp. 181–193, Apr. 2007. doi: 10.1016/j.probengmech.2006.11.002.

[5] S. P. Evans, D. R. Bradney, and P. D. Clausen, "Assessing the IEC simplified fatigue load equations for small wind turbine blades: How simple is too simple?" *Renew Energy*, vol. 127, no. 1, pp. 24–31, Nov. 2018. doi: 10.1016/j.renene.2018.04.041.

[6] Z. L. Mahri, M. S. Rouabah, and Z. Said, "Aeroelastic simulation of wind turbine blades," *Lect. Notes. Electr. Eng.*, vol. 11, pp. 313–323, May 2009. doi: 10.1007/978-0-387-76483-2.

[7] Z. L. Mahri and M. S. Rouabah, "Calculation of dynamic stresses using finite element method and prediction of fatigue failure for wind turbine rotor, WSEAS Trans," *Appl. Theor. Mech.*, vol. 3, no. 1, pp. 28–41, Jan. 2008.

[8] T. R. Liu and Y. S. Ren, "Vibration and flutter of wind turbine blade modeled as anisotropic thin-walled closed-section beam," *Sci. China Technol. Sci.*, vol. 54, no. 3, pp. 715–722, Mar. 2011. doi: 10.1007/s11431-010-4230-y.

[9] T. R. Liu, Y. S. Ren, and X. H. Yang, "Nonlinear aeroelastic stability analysis of wind turbine blade with bending-bending-twist coupling," *J. Fluid Struct.*, vol. 42, no. 23, pp. 488–502, Oct. 2013. doi: 10.1016/j.jfluidstructs.2013.08.006.

[10] F. Georgiades, J. Latalski, and J. Warminski, "Equations of motion of rotating composite beam with a nonconstant rotation speed and an arbitrary preset angle," *Meccanica*, vol. 49, no. 8, pp. 1833–1858, Aug. 2014. doi: 10.1007/s11012-014-9926-9.

[11] J. Warminski, L. Kloda, J. Latalski, A. Mitura, and M. Kowalczuk, "Nonlinear vibrations and time delay control of an extensible slowly rotating beam," *Nonlinear Dynam.*, vol. 103, no. 4, pp. 3255–3281, Mar. 2021. doi: 10.1007/s11071-020-06079-3.

[12] L. Li, Y. H. Li, Q. K. Liu, and H. W. Lv, "A mathematical model for horizontal axis wind turbine blades," *Appl. Math. Model.*, vol. 38, no. 11–12, pp. 2695–2715, Jun. 2014. doi: 10.1016/j.apm.2013.10.068.

[13] D. Y. Chen, C. J. Gu, P. Marzocca, J. D. Yang, and G. Pan, "Dynamic modeling of rotating blades system based on transfer matrix method of multibody system," *Appl. Math. Model.*, vol. 105, pp. 475–495, May 2022. doi: 10.1016/j.apm.2021.12.039.

[14] S. F. Fu et al., "Study on aerodynamic performance and wake characteristics of a floating offshore wind turbine under pitch motion," *Renew Energy*, vol. 205, no. 1, pp. 317–325, Mar. 2023. doi: 10.1016/j.renene.2023.01.040.

[15] L. Cottura, R. Caradonna, R. Novo, A. Ghigo, G. Bracco and G. Mattiazzo, "Effect of pitching motion on production in a OFWT," *J. Ocean Eng. Mar. Ener.*, vol. 8, no. 3, pp. 319–330, Aug. 2022. doi: 10.1007/s40722-022-00227-0.

[16] W. Y. Shi, J. Jiang, K. Sun, and Q. Y. Ju, "Aerodynamic performance of semi-submersible floating wind turbine under pitch motion," *Sustain. Energy Technol. Assess.*, vol. 48, pp. 101556, Dec. 2021. doi: 10.1016/j.seta.2021.101556.

[17] X. Shen, X. C. Zhu, and Z. H. Du, "Load control and unsteady aerodynamics for floating wind turbines," *Proc Inst. Mech. Eng. Part A J. Power Eng.*, vol. 235, no. 6, pp. 1501–1526, Sep. 2021. doi: 10.1177/0957650921993255.

[18] Z. W. Li, B. R. Wen, X. J. Dong, X. H. Long, and Z. K. Peng, "Effect of blade pitch control on dynamic characteristics of a floating offshore wind turbine under platform pitching motion," *Ocean Eng.*, vol. 232, no. 1, pp. 109109, Jul. 2021. doi: 10.1016/j.oceaneng.2021.109109.

[19] H. Boudounit, M. Tarfaoui, D. Saifaoui, and S. El Garouge, "Structural design of offshore wind turbine blade spars," *Wind Eng.*, vol. 46, no. 2, pp. 343–360, Apr. 2022. doi: 10.1177/0309524X211027812.

[20] O. Lagdani, M. Tarfaoui, M. Nachtane, M. Trihi, and H. Laaouidi, "Modal analysis of an iced offshore composite wind turbine blade," *Wind Eng.*, vol. 46, no. 1, pp. 134–149, Feb. 2022. doi: 10.1177/0309524X211011685.

[21] B. S. Kallesøe, "Equations of motion for a rotor blade, including gravity, pitch action and rotor speed variations," *Wind Energy*, vol. 10, no. 3, pp. 209–230, May/Jun. 2007. doi: 10.1002/we.217.

[22] S. Q. Wang, C. Y. Li, Y. Zhang, F. M. Jing, and L. F. Chen, "Influence of pitching motion on the hydrodynamic performance of a horizontal axis tidal turbine considering the surface wave," *Renew. Energy*, vol. 189, no. 3, pp. 1020–1032, Apr. 2022. doi: 10.1016/j.renene.2022.03.062.

[23] T. R. Liu, C. L. Sun, K. Zhao, and A. L. Gong, "Amplitude control of stall-induced nonlinear aeroelastic system based on iterative learning control and unified pitch motion," *Energies*, vol. 15, no. 3, pp. 787, Feb. 2022. doi: 10.3390/en15030787.

[24] Y. H. La, Y. S. Nam, and S. J. Hoon, "Individual pitch control of NREL 5MW wind turbine blade for load reduction," *Trans. Korean Soc. Mech. Eng. A*, vol. 36, no. 11, pp. 1427–1432, Nov. 2012. doi: 10.3795/KSME-A.2012.36.11.1427.

[25] M. Moness and A. M. Moustafa, "Hybrid modelling and predictive control of utility-scale variable-speed variable-pitch wind turbines," *Trans Inst. Meas. Control.*, vol. 42, no. 9, pp. 1724–1739, Jun. 2020. doi: 10.1177/0142331219895117.

[26] M. Seyednia, M. Masdari, and S. Vakilipour, "The influence of oscillating trailing-edge flap on the dynamic stall control of a pitching wind turbine airfoil," *J. Braz. Soc. Mech. Sci. Eng.*, vol. 41, no. 4, pp. 1–15, Apr. 2019. doi: 10.1007/s40430-019-1693-z.

[27] M. S. Mahmoud and M. O. Oyedeji, "Continuous-time multi-model predictive control of variable-speed variable-pitch wind turbines," *Int. J. Syst. Sci.*, vol. 49, no. 11, pp. 2442–2453, Aug. 2018. doi: 10.1080/00207721.2018.1505001.

[28] C. Rainone, D. De Siero, L. Iuspa, A. Viviani, and G. Pezzella, "A numerical procedure for variable-pitch law formulation of vertical-axis wind turbines," *Energies*, vol. 16, no. 1, pp. 536, Jan. 2023. doi: 10.3390/en16010536.

[29] A. Sagharichi, M. Zamani, and A. Ghasemi, "Effect of solidity on the performance of variable-pitch vertical axis wind turbine," *Energy*, vol. 161, no. 5, pp. 753–775, Oct. 2018. doi: 10.1016/j.energy.2018.07.160.

[30] L. Li, I. Chopra, W. D. Zhu, and M. L. Yu, "Performance analysis and optimization of a vertical-axis wind turbine with a high tip speed ratio," *Energies*, vol. 14, no. 4, pp. 996, Feb. 2021. doi: 10.3390/en14040996.

[31] C. Sendi, "Control of a variable blade pitch wind turbine subject to gust wind and actuators saturation," *Appl. Sci.*, vol. 11, no. 17, pp. 7865, Sep. 2021. doi: 10.3390/app11177865.

[32] J. C. Houbolt and G. W. Brooks, "Differential equations of motion for combined flapwise bending, chordwise bending, and torsion of twist nonuniform rotor blades," in *Technical Note 3905*, Washington, DC, USA, NACA, 1957.

[33] D. H. Hodges and E. H. Dowell, "Nonlinear equations of motion for the elastic bending and torsion of twisted nonuniform rotor blades," in *Technical Note D-7818*, Washington, DC, USA, NASA, 1974.

[34] L. Meirovitch, *Computational Methods in Structural Dynamics* (In Chinese). Beijing, China: National Defense Industry Press, 1987.

[35] A. H. Nayfeh and D. T. Mook, *Nonlinear Oscillations* (In Chinese). Beijing, China: Higher Education Press, 1980.

[36] W. Lacarbonara, H. Arvin, and F. Bakhtiari-Nejad, "A geometrically exact approach to the overall dynamics of elastic rotating blades—Part 1: Linear modal properties," *Nonlinear Dynam.*, vol. 70, no. 1, pp. 659–675, Oct. 2012. doi: 10.1007/s11071-012-0486-z.

[37] H. Arvin and F. Bakhtiari-Nejad, "Non-linear modal analysis of a rotating beam," *Int. J. Nonlin. Mech.*, vol. 46, no. 6, pp. 877–897, Jul. 2011. doi: 10.1016/j.ijnonlinmec.2011.03.017.

[38] H. Kim, H. Hee Yoo, and J. Chung, "Dynamic model for free vibration and response analysis of rotating beams," *J. Sound Vib.*, vol. 332, no. 22, pp. 5917–5928, Oct. 2013. doi: 10.1016/j.jsv.2013.06.004.